Cleaning of a model food soil from horizontal plates by a moving vertical water jet

D.I. Wilson[1,*], H. Köhler[2], L. Cai[1], J.-P. Majschak[2,3], and J.F. Davidson[1]

[1]Department of Chemical Engineering & Biotechnology, University of Cambridge, New Museums Site, Pembroke Street, Cambridge, CB2 3RA, UK

[2]Technische Universität Dresden, Faculty of Mechanical Engineering, Institute of Processing Machines and Mobile Machines, Bergstraße 120, 01062 Dresden, Germany

[3]Fraunhofer IVV, Branch Lab for Processing Machinery and Packaging Technology AVV, Heidelberger Straße 20, 01189 Dresden, Germany

Submitted to

Chemical Engineering Science

October 2014

Corresponding author

Dr D. Ian Wilson

Department of Chemical Engineering & Biotechnology
New Museums Site
Pembroke Street
Cambridge
CB2 3RA
UK

Tel +44 (0)1223 334791
E-mail diw11@cam.ac.uk

Cleaning of a model food soil from horizontal plates by a moving vertical water jet

D.I. Wilson[1,*], H. Köhler[2], L. Cai[1], J.-P. Majschak[2,3], and J.F. Davidson[1]

[1]Department of Chemical Engineering & Biotechnology, University of Cambridge, New Museums Site, Pembroke Street, Cambridge, CB2 3RA, UK

[2]Technische Universität Dresden, Faculty of Mechanical Engineering, Institute of Processing Machines and Mobile Machines, Bergstraße 120, 01062 Dresden, Germany

[3]Fraunhofer IVV, Branch Lab for Processing Machinery and Packaging Technology AVV, Heidelberger Straße 20, 01189 Dresden, Germany

Abstract

The removal of layers of a model food soil (dried Xanthan gum containing fluorescent ZnS particles) by a vertical water jet impinging normally on to the plate, generated by a solid stream nozzle which moves across the plate was reported by Köhler *et al*. (2014). Their experiments investigated nozzle pressures from 0.5-2.0 barg; nozzle diameters from 0.84-2.66 mm, nozzle-layer separation of 20 mm, and nozzle traverse speeds of 2.1-126 mm s^{-1}. The flow parameters and separation are smaller than those typical of industrial jet cleaning operations.

The model developed by Wilson *et al*. (2014; *Chem. Eng. Sci*., **109**, 183–196) for cleaning of similar layers by a stationary impinging jet was modified to describe the case of moving nozzle. This new model predicted the trends observed in the experiments, and analysis of the data yielded a similar cleaning rate constant to that obtained previously for cleaning of similar layers by stationary jets. The model predicted a non-circular cleaning front which matched that extracted from new experiments in which the flow was interrupted in order to capture this feature. The model allowed the cleaning performance indicators suggested by Köhler *et al*. (2014) to be expressed quantitatively: these indicated that higher nozzle traverse speeds give increased cleaning time, energy and liquid consumption performance.

Keywords Cleaning; impinging jet; moving jet; productivity; Xanthan gum

Introduction

Efficient cleaning is critically important for sustainable manufacturing, whether to clear residual material from process lines in multi-product plant (Palabiyik *et al*., 2014) to avoid cross-contamination or to remove fouling deposits that reduce operating performance and/or threaten product quality (Wilson, 2005; Fryer and Asteriadou, 2009). In the process industries, and particularly the food and pharmaceuticals sector, cleaning is commonly achieved by cleaning-in-place operations whereby aqueous solutions are circulated through units and remove residual films by a combination of thermodynamics (*i.e*. temperature, dissolution), mechanics (hydraulic action of the flow) and chemistry (surfactants, detergents, dispersants and reactive agents). The environmental impact, in

terms of water (consumption, treatment and discharge of treated streams), and energy demand of such operations is large (Burfoot and Middleton, 2009): estimates of water consumption in dairy processing range from 1.5-2.5 m^3 per m^3 milk processed (Carbon Trust, 2011) and in the brewing sector estimates range from 3.9-6.3 m^3 per m^3 beer processed (Hien *et al.*, 2008).

The need to improve the efficiency of cleaning-in-place operations for tanks and other process vessels has promoted the move away from simple 'fill, soak and dump' strategies to the use of impinging jets generated by rotating spray balls, moving nozzles, robotic lances *etc*. The hydraulic forces imparted by the jet increase the local rate of cleaning over simple soaking or agitation methods, albeit with an associated increase in energy input and capital cost. Static spray balls are effective for wetting surfaces but are less effective for cleaning because the points of impingement, where the largest hydraulic forces are generated, are at fixed locations on the tank wall.

There is a good understanding of cleaning of surface layers by impinging liquid jets involving dissolution mechanisms, where thermodynamics (solubility) and convective mass transfer from the surface determine the cleaning rate. The underlying flow problem is of particular interest to fluid mechanicists as the flow regime near the point of impingment approximates a Holman flow (reference). Similarly, the cleaning of surfaces by particles entrained in a moving fluid, *e.g*. sandblasting, where the particulates are an erodent (*e.g*. Momber, 2008), has been studied at length. Cleaning by other mechanisms has received less attention in the literature. Yeckel and Middelman (1987) studied the removal of a mobile fluid coating (a Newtonian oil) by a stationary impinging jet, while Fuller and co-workers (Hsu *et al*., 2011; Walker *et al*., 2012) studied the removal of non-Newtonian fluid layers using stationary jets: both require solution of a coupled flow problem involving the jet liquid and the complex fluid in the layer. Walker *et al*. (2014) demonstrated that the stresses induced in a non-Newtonian coating could be exploited to remove particulate material from the underlying substrate more effectively than using Newtonian liquids. Cleaning of soft solid layers by moving jets has received little attention, with the exception of the work on sprays by Leu *et al*. (1998) and Meng *et al*. (1998) and applications of high speed jets to remove harder layers (decoating), *e.g*. Mabrouki *et al*. (2000). Burfoot and Middelton (2009) and Burfoot *et al*. (2009) reported investigations of the removal of biofilms and stubborn soils by high pressure jets, but related their results solely to the pressure imposed on the surface being cleaned. Removal in these studies was not strongly related to pressure: the use of detergent was more significant.

The primary operating variables in impinging jet cleaning, apart from the properties of the soil to be removed (which largely dictates the chemistry and temperature of the cleaning liquid to be used), are the nozzle diameter, d_N, pressure drop across the nozzle, ΔP, and the speed at which the nozzle moves across the surface, v_{jet}. The distance from the nozzle to the wall is also important as this determines

the extent to which the jet breaks up in flight and also the traverse speed for a jet generated by a rotating nozzle. Köhler *et al*. (2014) reported a series of experimental studies of the removal of a model food soil (dried layers of Xanthan gum containing fluorescent ZnS crystals) by a moving, vertical water jet where the effect of the above parameters on the rate of cleaning, expressed as the width of the region cleared by the jet, w_c, was investigated. They reported an empirical relationship between w_c and operating parameters d_N, ΔP, and v_{jet}. The traverse speeds (up to 120 mm s^{-1}) and water pressures (up to 2 barg) investigated are lower than those employed in industry for jet cleaning (speeds of several m s^{-1} and pressures of around 5 barg, respectively) and there are some fluid flow phenomena which affect scale-up of their results to industrial practice. Some of these are discussed later in this paper.

This paper reports a mathematical model for cleaning by a moving vertical jet which gives good agreement with the results reported by Köhler *et al*. as well as a short series of further experiments where cleaning was interrupted, in order to establish the shape of the cleaning front. The model is based on that reported by Wilson *et al.* (2014) for cleaning soil layers via adhesive failure by a stationary vertical jet, which described the removal of the model food soil employed by Köhler *et al*. in addition to other soft solid layers (dried polyvinylalcohol (PVA) glue and Vaseline®). The cleaning rate constant reported in the stationary jet studies is found to give a good quantitative description of the behaviour observed with moving jets.

Model

Stationary impinging jets

In the Wilson *et al*. (2014) model for removal of thin soil layers by stationary impinging liquid jets by adhesive failure, the force imposed by the spreading liquid film in the radial flow zone (see Figure 1) is sufficient to detach the soil from the substrate. This model is now applied to the case where the point of jet impingement is moving over a soiled substrate, at constant traversing velocity v_{jet}.

Flow behaviour

Figure 1 is a schematic of the fluid flow patterns created by a liquid jet impinging normally on a substrate. In the case of *vertical* jets impinging *downwards* on a *horizontal* substrate, the liquid flows radially outwards with mean velocity U at distance r from the point of impingement until the point where the film changes thickness abruptly, giving a hydraulic jump, at radius R_H. Beyond the hydraulic jump the liquid flows radially outwards, slowly. With a *horizontal* jet impinging on a *vertical* plate, a similar radial flow zone is formed until a distance R_F, where a film jump is formed and the liquid velocity again decreases markedly. Beyond the film jump, however, the liquid forms a circumferential rope and drains vertically downwards under gravity. The flow patterns associated with

the film jump and models for predicting its size and behaviour are described in Wilson *et al*. (2012) and Wang *et al*. (2013a).

Within the radial flow zone, at $r_o < r < R$, where R refers to R_H or R_F, the mean velocity in the liquid film, U, in both cases (ignoring gravity) is given by

$$\frac{1}{U} = \frac{1}{U_o} + \frac{10\pi^2 \rho\mu}{3\dot{m}^2}\left(r^3 - r_o^3\right) \quad [1]$$

where $\dot{m}$ is the mass flow rate of liquid in the jet, r_o is the radius of the jet, ρ is the liquid density, μ its viscosity, and U_o the initial film mean velocity.

Equation [1] indicates that U decreases as r increases. If U_o^{-1} is small (discussed by Wang *et al*., 2013b), this gives

$$\frac{1}{U} = \frac{10\pi^2 \rho\mu}{3\dot{m}^2}\left(r^3 - r_o^3\right) = \frac{c}{\dot{m}^2}\left(r^3 - r_o^3\right) \quad [2]$$

where c is a group of parameters: for water at 20˚C, $c = 10\pi^2\rho\mu/3 = 32.9$ kg^2 m^{-4} s^{-1}. The flow rate of momentum per unit length of circumference, M, (a momentum flux) is given by (Wilson *et al*., 2012)

$$M = \frac{3\dot{m}}{5\pi}\frac{U}{r} \quad [3]$$

Adhesive removal

When a stationary jet causes adhesive removal, the flow creates a circular clean region of radius a which increases in size over time, t. Wilson *et al*. (2014) proposed that the rate of adhesive removal (peeling, fragmenting) of a film of thickness δ is proportional to the rate of flow of momentum in the liquid film at a, *viz*.

$$\frac{da}{dt} = kMf(\delta) \quad [4]$$

where k is a cleaning rate constant. Equation [4] states that the force driving peeling is a fraction of the maximum force which could be imparted by the liquid flow: $f(\delta)$ is some functional dependency on soil layer thickness and rheology which has yet to be elucidated, so a lumped cleaning rate constant, k', is used. Setting r equal to a, with M and U calculated using Equations [4] and [3], respectively, gives

$$\frac{da}{dt} = k'M = k'\frac{3}{5\pi}\frac{\dot{m}^3}{c}\frac{1}{a\left(a^3 - r_o^3\right)} \quad [5]$$

Integrating Equation [5] from the point where adhesive breakthrough is first noticed, a_i, at time t_i, to time t gives

$$\left[\frac{a^5}{5}-r_o^3\frac{a^2}{2}\right]_{a_i}^{a}=\frac{3k'}{5\pi c}\dot{m}^3\left(t-t_i\right) \quad [6]$$

When $a_i > r_o$, such that $a^5 \gg r_o^3 a^2$, Equation [6] reduces to

$$a\approx\sqrt[5]{\frac{3k'}{\pi c}\dot{m}^3}\times\left(t-t_i\right)^{1/5}=K\Delta t^{0.2} \quad [7]$$

and Equation [5] gives

$$\frac{da}{dt}=k'\frac{3}{5\pi}\frac{\dot{m}^3}{c}\frac{1}{a^4} \quad [8]$$

Equation [7] describes the evolution of the cleared area by a stationary jet for $a < R_{H/F}$, *i.e*. within the radial flow zone. Equation [8] is used here to describe the removal rate for a moving jet. Equations [7] and [8] apply where $a^3 \gg r_o^3$, and there is little influence of the jet radius. Near the point of impingement Equation [1] does not give an accurate prediction of the mean velocity in the film owing to the growth of a boundary layer in the speading film. Moreover, in the vicinity of the region where the jet strikes the wall, cleaning will be dominated by impact forces, which are related to the momentum flow rate (pressure) in the jet.

Figure 2 shows the extent of removal of horizontal Xanthan gum/ZnS layers similar to those studied in the moving jet experiments reported here by stationary water jets, for two nozzle sizes and a common feed water pressure of 1.5 barg. These data sets were collected during the study reported by Köhler *et al*. (2013). The radius of the cleaned layer is plotted against $\Delta t^{0.2}$, as suggested by Equation [7], giving strongly linear trends for two of the cases, from which k' can be estimated as 0.0053 ± 0.0006 and 0.0022 ± 0.0005 s m kg^{-1} for d_N = 1.69 and 2.66 mm, respectively. These values are consistent with the average k' value of 0.002 m s kg^{-1} reported by Wilson *et al*. (2014) for a data set of similar layers in over 40 tests: this provides an indication of the sensitivity of these films to batchwise variations and small differences in preparation protocols over time. The non-linearity of the second 2.66 mm nozzle (labelled d_N = 2.66 mm (*b*)) profile is attributed to non-uniformity in the coating, which is an issue in preparing coatings on these large areas (0.5×0.5 m^2) but also representative of real layers. Separate experiments, where the relative humidity was controlled between 25% and 80% relative humidity at a dry bulb temperature of 23°C gave k' values between 0.0014 and 0.0024 m s kg^{-1}, indicating that humidity was not a significant factor with these materials in these tests.

Moving jets

Equations [3] and [5] indicate that the local rate of removal is strongly related to radial position. Beyond the hydraulic or film jump *U* is relatively low, and the rate of cleaning distant from the nozzle is subsequently small. The local liquid velocity beyond the jump is not currently predictable for

vertical plates so this analysis focuses on the case where removal takes place within the radial flow zone. The following analysis applies to jets impinging normally to the substrate: the flow behaviour of jets impinging obliquely has been reported by Wang *et al*. (2013b) and extension of this model to obliquely impinging moving jets is the subject of ongoing work.

If the liquid in the jet is moving significantly faster than the nozzle traverse speed, *i.e*. $U \gg v_{jet}$, the soil is effectively static with respect to the jet. The rate of removal of the soil is then determined by the radial distance from the impingement point. Consider the locations shown in Figure 3, which shows a photograph and schematic of the shape of the cleaned area when a traversing jet is interrupted (flow cut off). A video of the experiment is available as Supplementary Material A (d_N = 1.69 mm, ΔP = 1.5 bar, v_{jet} = 10.5 mm s^{-1}). The leading front of the cleaned zone is curved but it is not a circular arc. The cleaning front, *i.e.* the interface between the soiled and cleaned regions, is assumed to lie within the radial flow zone, which extends to the jump, radius R_H.

The relative motion of the point of impingement and the interface between the soiled and cleaned regions requires a vector analysis. Whereas the experiments featured the nozzle moving from left to right (Figure 3(a)), it is simpler to consider the jet frame of reference, Figure 3(b), where the point of impingement is stationary and the soil moves towards the point of impingement, O, from the right.

Point X, located a distance a_X directly ahead of the jet, is a stationary point where the rate of cleaning is equal to the rate at which material is convected towards this point, at v_{jet}. Substituting this condition into Equation [5], with $a_X \gg r_o$, gives

$$\frac{da}{dt} = v_{jet} = k' \frac{3}{5\pi} \frac{\dot{m}^3}{c} \frac{1}{a_X^4} = \frac{\alpha}{a_X^4} \qquad [9]$$

where α is a group of parameters. In Figure 4, at point P, where the interface is oriented at angle θ to the direction of nozzle movement, the rate of cleaning in the radial direction (OB) is given by $da/dt = \alpha/p^4$, where p is the radial distance from O to P (and varies with θ); this is based on the fact that the radial velocity of the liquid, U, is much greater than v_{jet}.

The vectors involved in cleaning at point P are shown in Figure 4. The angle ϕ defines the direction of the net motion of the interface in relation to the normal, PC, to the direction of v_{jet}: this direction of motion arises from two velocity vectors, namely *(i)* the vector $(\alpha/p^4) \cos(\theta - \phi)$, which is normal to the interface, added vectorially to (ii) the vector v_{jet} in the direction of motion of the jet.

At angle θ + dθ, dθ being infinitesimal in the usual calculus notation, the radial distance to the interface is p + dp. This defines the small triangle PQR, the angle PQR being, to first-order, a right angle. Thus

$$QR = dp = pd\theta \tan(\theta - \phi) \quad [10]$$

pdθ being the length PQ, infinitesimal.

The net motion of the interface, direction PR, arises from the combination of two vectors, namely (*i*) the vector (α/p^4) cos (θ - ϕ), the component normal to the interface, of the vector α/p^4 which is colinear with vector p, and (*ii*) the vector v_{jet}.

From the triangle ABP, it follows that the distance AC = v_{jet} - (α/p^4) cosθ and the distance PC = (α/p^4)sin θ, so the ratio

$$\frac{AC}{PC} = \tan(\phi) = \frac{v_{jet} - (\alpha/p^4)\cos\theta}{(\alpha/p^4)\sin\theta} \quad [11]$$

After eliminating ϕ from between Equations [10] and [11], with some simplification, it is readily shown that

$$\frac{dp}{d\theta} = \frac{\alpha}{v_{jet} p^3 \sin\theta} - \frac{p}{\tan\theta} \quad [12]$$

Integration of the first order non-linear differential Equation [12] gives the curve shown in Figure 5. The shape of the cleaning locus in Cartesian co-ordinates relative to the point of impingement, O, is obtained by calculating $x = p\cos\theta$, $y = p\sin\theta$ and is presented in dimensionless form, *i.e.* (x/a_x, y/a_x).

There is a maximum in the dimensionless half-width, at the point labelled W, with y/a_x = 1.47 at θ = 127° (x/a_x = -1.11; p/a_x = 2.22). This marks the widest point that is cleaned: the narrower front at larger θ values is not observed as the region will already have been cleaned by the passage of the jet upstream and, once cleaned, cannot be soiled again.

The cleared width, w_c, is then given by

$$w_c = 2 \times 1.47 a_x = 2.94 a_x = 2.94 \left\{ k' \frac{3}{5\pi} \frac{\dot{m}^3}{c} \frac{1}{v_{jet}} \right\}^{0.25} \quad [13]$$

The cleaning front is described by Figure 5 as long as the liquid velocity is relatively fast, which was the case for all the soil layers studied here. Some deviations were observed when the soil layer peeled off in large lumps, indicating non-uniform adhesion to the substrate.

The size of the cleaned zone changes less strongly downstream of the point of impingement. At O, where $\theta = 90°$, $x/a_x = 0$, the numerical integration referred to above gives $y/a_x = 1.28$. The value of p changes from $1.28a_x$ at O to $2.22a_x$ at W. One of the assumptions of the model is that the interface lies within the radial flow zone, *i.e.* $p \leq R_H$. It is possible that the cleaning front could reach the hydraulic jump at some point. The experimental data were checked for this condition: setting p at W (Figure 5) $\leq R_H$ requires $w_c \leq 1.32\ R_H$. Data not meeting this criterion were filtered from the set for comparison with Equation [13].

Equation [13] allows the width of the cleaned region to be calculated, or k' estimated. The mass flow rate through the nozzle is given by

$$\dot{m} = C_d \frac{\pi d_N^2}{4} \sqrt{2\rho\Delta P} \qquad [14]$$

where C_d is the nozzle discharge coefficient and d_N the nozzle diameter. Combining [13] and [14] yields the following relationship between the width of the cleaned region and the nozzle operating parameters:

$$w_c = 2.94\left[\frac{9}{3200}\frac{d_N^6}{\rho\mu} C_d^3 (2\rho\Delta P)^{1.5} \frac{k'}{v_{jet}}\right]^{0.25} = k'^{0.25} f(v_{jet}) \qquad [15]$$

Plots of w_c against f should be linear, with gradient $k'^{0.25}$.

Experimental

Soil and Substrate

Model food soil layers were prepared from solutions of Xanthan gum (a natural polysaccharide, supplied by Kremer Pigmente GmbH & Co. KG, Xanthan, CAS 11138-66-2) mixed with 30 g L^{-1} crystalline zinc sulphide (Honeywell, USA, Lumilux® Effect Green N-FF) as optical tracer. The Xanthan gum (5 g L^{-1}) was dissolved in distilled water (23 °C) and stirred at 600 rpm for 30 minutes. The tracer particles were then added and stirring continued for another 5 minutes until a well dispersed suspension was obtained.

The stainless steel test sheets (dimensions in mm, 500 × 500 × 1, AISI 304, 2B finish) were cleaned with water and ethanol before soiling. The sheets were placed upright and the test soil was sprayed on to give a homogeneous film. Excess solution flowed down off the plate, leaving a uniform, thin layer which was then dried at room temperature for 24 h. This protocol gave a mean surface mass coverage, $m_0 = 1.1 \pm 0.1$ mg/cm² ($n = 41$), measured gravimetrically.

Cleaning Test Rig

The coated sheets were cleaned using the apparatus in Figure 6. A vertical, coherent, round liquid jet is moved across the sheet so that the liquid impinged normally on the test section. The nozzle was driven by a linear axis device with adjustable traverse speed, setting v_{jet}. The test sheet was positioned with a slight inclination to the horizontal (< 1 °) to ensure a stable flow off the sheet. The jet was generated by solid stream nozzles (Lechler GmbH, Type 544). The distance between the nozzle and test sheet was maintained at 20 mm since earlier experiments showed that this parameter has negligible influence over the range where the jet remains coherent (Köhler *et al*., 2013). At longer separations, where the jet has started to split up, the flow patterns in the spreading liquid film will be unsteady and the influence of this on cleaning has yet to be established. Four different nozzle diameters d_N and a range of feed pressures were used: the conditions employed in the tests reported in Table 1. The nozzle discharge coefficient, C_d, was determined separately with bucket and stopwatch. The test liquid in all cases was deionised water, at a temperature of 22 ± 1.7 ºC and pH 6.

The phosphorescent zinc sulphide tracer in the soil layer was illuminated by two UVA lamps. The apparatus was located within a light-tight box to maintain constant lighting conditions. A PC controlled the pump pressure, flow, linear axis position and collected sensor data. Once cleaning was completed an image of the test sheet was taken manually with a digital camera (Olympus TG-630, 12 megapixel). Cleaning was interrupted by stopping the water flow in a small subset of tests in order to generate images of the shape of the cleaning front.

Data Analysis

Images were analysed automatically by a MATLAB® script (see Figure 7). The image was first cropped to the region of interest to avoid side effects. The maximum emission of the tracer occurs at 530 nm so only the green values of the RGB image were employed for detecting the boundary between the cleaned and uncleaned area. The image is converted to a binary array using the MATLAB® functions *graythresh* and *im2bw*. The cleaned width, w_c, was obtained by smoothing and averaging the distance between the edges over the hole track.

Experiments

The movement of the nozzle normally started before, and terminated after, the edge of the test sheet to ensure constant speed as it traversed the sheet. Video recordings were obtained by attaching the camera to the nozzle traverse bar. 72 tests were performed for 47 different experiments, including several repeats. Experimental reproducibility was good (*e.g.* $w_c = 52 \pm 4$ mm for 7 experiments with $d_N = 1.69$ mm, $\Delta P = 1.5$ barg, $v_{jet} = 10.5$ mm s^{-1}). The operating parameters studied, summarised in Table 1, were selected using design of experiments principles. The jet was always turbulent, with Reynolds numbers in the range $7.7 \times 10^3 \leq Re_{jet} \leq 5.0 \times 10^4$.

Results and Discussion

All the video records indicated that the cleaning front was roughly elliptical, as shown in Figure 5, as predicted by the model. Figure 8 compares the mean film velocity at the leading edge of the cleaning front, at point X on Figure 3(*b*), to the jet velocity. Calculation of $U(a_x)$ using Equation [2] requires an estimate of the jet radius, from $r_o \approx d_N/2$, and a_x, taken from $w_c = 2.94a_x$ (see Equation [13] and Figure 5). The plot shows that the nozzle traverse speed is over two orders of magnitude less than $U(a_x)$: there is no systematic trend. The relative velocity of the liquid in the film to the substrate can therefore be assumed to have little effect.

One of the assumptions of the model is that the cleaning front lies within the radial flow zone, so that the momentum flow rate can be estimated using Equation [3]. The radius of the hydraulic jump was estimated using the result from Wilson *et al*. (2012)

$$R = 0.276\left[\frac{\dot{m}^3}{\mu\rho\gamma(1-\cos\beta)}\right]^{1/4} \qquad [16]$$

where γ is the liquid/air surface tension and β the contact angle, with values 0.073 N m^{-1} and 98°, respectively (Köhler *et al*., 2014). Figure 9 shows that this assumption was valid for most of the test cases. The 18 cases where this assumption did not hold, most of which were obtained at the lowest nozzle speed, were excluded from further comparisons. This exclusion criterion assumed that Equation [16] gave an predicted *R* accurately: it will be shown that many of the excluded data sets fitted the model well.

The shapes of the cleaning front were extracted from interrupted experiments and two examples are plotted in dimensionless form alongside the model prediction in Figure 5. The scaling length, a_x, for each case was calculated from $w_c = 2.94a_x$.The plots show very good agreement with the model, within the estimates of experimental uncertainty. This indicates that the assumptions of the cleaning model, which were developed using tests with stationary jets, translate successfully to the moving case. This represents a 'classical' piece of chemical engineering analysis, where results from batch experiments are used to describe a continuous operation.

The cleaning model, Equation [13], predicts a linear relationship between w_c and $v_{jet}^{-0.25}$. A decreasing trend is apparent in Figure 9. The influence of nozzle diameter was removed by plotting the data in the form of Equation [15]. Figure 10 shows very good agreement with the model. Linear regression gave the gradient, $k'^{0.25}$, as 0.2115 (m s kg^{-1})$^{0.25}$ with regression coefficient R^2 = 0.846. This corresponds to $k' = 0.2115^4 = 0.0020$ m s kg^{-1}, which is similar to the values obtained from the batch

experiments presented in Figure 2 and the value reported by Wilson *et al*. (2014). This result provides further quantitative confirmation of the model.

The data in Figure 10 are distributed randomly about the line of best fit. The open symbols indicate data where the p at W < R_H criterion was not satisfied. The reliability of the model in these cases is then uncertain as the estimate of M is based on the result for the radial flow region (Equation [2]). The data nonetheless follow the general trend, indicating that the model gives a reasonable prediction for these cases. This is attributed both to (*i*) the R_H values being themselves estimates (and thus subject to some uncertainty), and the (*ii*) the width of the cleaning front does not increase by a large amount downstream of the point of impingement, where dimension p increases strongly (see Figure 5: y = 1.28 a_x at x = 0 *cf*. y = 1.47 a_x at W). There is a suggestion of a systematic difference between the predicted and experimental values at higher v_{jet} values with d_N = 1.69 mm, marked E on Figure 10. The model appears to overpredict these values. Modifying the model prediction to include the effect of r_o and U_o (via Equations [1] and [2]) did not improve the agreement and this represents a topic for further work. Phenomena such as splashback, reported by Wang *et al*. (2013b), and impact erosion may be important.

A second topic for further work is the extension of the model to oblique jets, *i.e*. ones that impinge on the surface at angles other than 90°. This is important for tank cleaning applications, as rotation of the spray nozzle in order to achieve complete coverage of the tank internals will result in the impingement angles varying with location on the tank wall. The momentum flow rate, M, will then vary with azimuthal position on the plate, θ, and Equation [5] will be a more complicated function of θ. The flow behaviour in the radial flow zone for obliquely impinging jets was studied by Wang *et al*. (2013b, 2014) and their model for the flow can be combined with the cleaning model presented here.

A third topic, of particular relevance to industrial jet cleaning applications, is that of geometrical scale-up. The tests considered here all featured coherent impinging jets, which gave quasi-stationary liquid flow patterns on the wall. Larger separations, of order 1-2 m, are likely to give rise to jet breakup, unsteady flow across the wall, and lower impact forces at the point of impingement. With a rotating nozzle, larger separations will also increase the traverse speed and give a curved jet trajectory. Industrial cleaning operations also tend to employ higher liquid flow rates.

Performance Indicators

A number of methods for quantifying the efficiency of cleaning by impinging jets exist, as discussed by Köhler *et al*. (2014), differing in terms of the resource employed to achieve cleaning. For instance, higher jet velocities generally increase the rate of cleaning but require larger liquid flow rates and

energy input. The cleaning model is used here to evaluate the measures discussed by Köhler *et al*. (2014) and to identify general trends. The different indicators, framed in terms of the above variables, are

(*i*) Time-based cleaning, E_t:

$$E_t = \frac{\text{soil mass removed}}{\text{cleaning time}}: \quad E_t \propto w_c v_{jet} \qquad [17]$$

Inserting the result for w_c in equation [15] gives

$$E_t \propto d_N^{1.5} \Delta P^{0.375} v_{jet}^{0.75} \qquad [18]$$

(*ii*) Liquid consumption, E_V

$$E_V = \frac{\text{soil mass removed}}{\text{volume of cleaning solution}}: \quad E_V \propto \frac{w_c v_{jet}}{\dot{m}/\rho} \qquad [19]$$

Substituting for w_c gives

$$E_V \propto \frac{v_{jet}^{0.75}}{d_N^{0.5} \Delta P^{0.125}} \qquad [20]$$

(*iii*) Hydraulic energy consumption, E_E

$$E_E = \frac{\text{soil mass removed}}{\text{energy consumed}}: \quad E_E \propto \frac{w_c v_{jet}}{\Delta P \times \dot{m}/\rho} \qquad [21]$$

It should be noted that this parameter does not include the work required to move the nozzle. This gives

$$E_E \propto \frac{v_{jet}^{0.25}}{d_N^{0.5} \Delta P^{1.125}} \qquad [22]$$

Inspection of the above results, Equations [18], [20] and [22], yields increasing trends with v_{jet} but differing dependencies on d_N and ΔP. All three performance indicators increase with increasing v_{jet}, suggesting that the nozzle traverse speed should be as high as possible, but the caveat identified from the data sets in Figure 10 means that there may be a change in sensitivity at higher v_{jet} and this needs to be confirmed. Limits to v_{jet} arise in industrial practice, where jet throw length is determined by jet breakup and curved trajectories. The three indicators differ noticeably in their dependency on flow rate and pressure drop: E_t increases with both, more strongly with d_N. E_V and E_E decrease with both, with a common dependency on d_N: E_V is almost insensitive to ΔP while E_E is noticeably more sensitive.

The dependency of these performance indicators on design and operating variables is demonstrated in Figure 11, which is a 3-dimensional plot with E_t as the *z* co-ordinate and E_V and E_E as the *x* and *y* co-ordinates, respectively. This scheme was chosen as time-based effectiveness is likely to the primary

performance indicator in industrial practice. The values of E_t, E_V and E_E were evaluated using the properties of the soil and liquid employed in the experiments, *e.g.* $k' = 0.0020$ m s kg^{-1} and a surface coverage of 11 g m^{-2}. The E_E calculation employed a pump efficiency of 76% and a (lab scale) motor efficiency of 85%: pressure losses due to fittings and work or liquid used to move the jet were not considered. The effect of varying design parameters d_N, v_{jet} and ΔP was explored across the design space by plotting three loci, which intersected at the base case, marked S, at which $d_N = 1.69$ mm, $\Delta P = 1.5$ bar, and $v_{jet} = 21$ mms^{-1}. The loci covered the range relevant to this study, *viz*.

(i) Constant d_N and $\Delta P = 1.5$ bar, v_{jet} varied from 2 - 130 mm s^{-1};

(ii) Constant d_N and v_{jet}, ΔP varied from 0.5-5.0 bar;

(iii) Constant ΔP and v_{jet}, d_N varied from 0.39 - 3.3 mm.

The dependencies described qualitatively above are evident in the plots. It is noticeable that all three performance indicators increase as v_{jet} is increased, whereas increasing ΔP gives a modest benefit in E_t but is accompanied by a large reduction in E_E. Increasing d_N over the range gives over an order of magnitude benefit in E_t but poorer E_E and E_V performance. These results confirm the need for further work to investigate the differences between the model and experimental data at higher v_{jet} values.

Conclusions

The model developed previously for cleaning soiling layers from solid substrates by a stationary vertical impinging liquid jet was modified to describe cleaning by a similar mechanism by a moving vertical jet. The model reproduced the relationships between cleaned region width, nozzle diameter, nozzle pressure and jet traverse velocity observed in the moving jet experiments reported by Köhler *et al*. (2014). The value of the cleaning rate parameter, k', calculated from the data for removal of the Xanthan gum/ZnS layers by moving jets was very similar to that calculated previously for cleaning similar layers by stationary impinging liquid jets. Further evidence of the veracity of the model was that the shape of the removal zone near the point of jet impact, determined by new, interrupted experiments, was in very good agreement with that predicted by the model.

The model allowed the cleaning performance indicators proposed by Köhler *et al*. (2014) to be expressed in a quantitative form. This indicated that the use of higher jet traversing speeds give increased productivity in terms of rate of cleaning, energy requirement and liquid consumption per unit mass of soil removed.

Acknowledgements

The work at TU Dresden was funded by the European Union and the Free State of Saxony as part of project SAB 080951793. A short vacation study grant for LC from Fitzwilliam College, Cambridge, is gratefully acknowledged. The reviewers provided several helpful insights into industrial applications.

References

Burfoot, D. and Middelton, K. (2009) Effects of operating conditions of high pressure washing on the removal of biofilms from stainless steel surfaces, *J. Food Eng*., **90**, 350-357.

Burfoot, D., Middelton, K. and Holah, J.T. (2009) Removal of biofilms and stubborn soil by pressure washing, *Trends Food Sci. Tech*., **20**, S45-S47.

Carbon Trust (2011) *Industrial Energy Efficiency Accelerator. Guide to the Dairy Sector*, Report CTG033. Carbon Trust, UK.

Fryer, P.J., Asteriadou, K. (2009) A prototype cleaning map: a classification of industrial cleaning processes. *Trends in Food Science & Technology*, **20**, 225–262.

Hsu, T.T., Walker, T.W., Frank, C.W. and G. G. Fuller, G.G. (2011) Role of fluid elasticity on the dynamics of rinsing flow by an impinging jet, *Phys. Fluids*. **23**, 033101.

Hien, O., Küpferling, E., Guggeis, H. (2008) Wassermangement in der Getränkeindustrie, *Brauwelt*, **23**, 640-643.

Jensen, B.B.B. (2011), Tank cleaning technology: Innovative application to improve clean-in-place (CIP), EHEDG Yearbook 2011/2012, 26-30.

Köhler, H., Stoye, H., Mauermann, M. and Majschak, J.-P. (2013) Optimization Approach for efficient cleaning with impinging jets – influence of nozzle diameter, pressure and nozzle distance, Proc. Xth Intl. Conf. on Heat Exchanger Fouling and Cleaning, Budapest, www.heatexchanger-fouling.com/papers/papers2013/61_Koehler_F.pdf.

Köhler, H., Majschak, J-P., (2014) Cleaning efficiency - which efficiency? Study of the influences of nozzle diameter, pressure and jet moving speed of impinging jets, *Food & Bioproducts Processing*, under review.

Leu, M.C., Meng, P., Geskin, E.S., Li, F. Tismenenskiy, L. (1998) Mathematical modelling and experimental verification of stationary waterjet cleaning process, *J. Manuf. Sci. Eng*., **120**, 571-579.

Mabrouki, T., Raissi, K. and Cornier, A. (2000) Numerical simulation and experimental study of the interaction between a pure high-velocity waterjet and targets: contribution to investigate the decoating process, *Wear*, 239(2), 260-273.

Meng, P., Geskin, E.S., Leu, M.C., Li, F. Tismenenskiy, L. (1998) An analytical and experimental study of cleaning with moving waterjets, *J. Manuf. Sci. Eng*., **120**, 580-589.

Momber, A. (2008) *Blast Cleaning Technology*, Springer.

Palabiyik, I., Olunloyo, B., Fryer, P..J and Robbins, P.T. (2014) Flow regimes in the emptying of pipes filled with a Herschel-Bulkely fluid, *Chem. Eng. Res. Des*., in press, doi: 10.1016/j.cherd.2014.01.001.

Patel, S. and Jordan, W.K. 1970, Studies of flow dynamics of falling films of water and its effect on cleaning of stainless steel, *J. Food Sci.*, **35**, 374-377.

Schöler, M., Fuchs, T., Helbig, M., Augustin, W., Scholl, S. and Majschak, J.-P. (2009). Monitoring of the local cleaning efficiency of pulsed flow cleaning procedures, Proc. 8th Int. Conference on Heat Exchanger Fouling and Cleaning 2009, Schladming, Austria, pp. 455–463.

Walker, T.W., Hsu, T.T., Frank, C.W. and Fuller, G.G. (2012) Role of shear-thinning on the dynamics of rinsing flow by an impinging jet, *Phys. Fluids*, **24**, 093102.

Walker, T.W., Hsu, T.T., Fitzgibbon, S., Mui, D.S.L., Zhu, J., Mendiratta, A., Frank, C.W., Fuller, G.G. (2014) Surface cleaning and particle removal using non-Newtonian liquids. *J. Rheol*. **58**, 63 (2014).

Wang, T., Davidson, J.F. and Wilson, D.I. (2013a) Effect of surfactant on flow patterns and draining films created by a static horizontal liquid jet impinging on a vertical surface, *Chem. Eng. Sci*., **88**, 79-94.

Wang, T., Faria, D., Stevens, L.J., Tan, J.S.C., Davidson, J.F. and Wilson, D.I. (2013b) Flow patterns and draining films created by horizontal and inclined water jets impinging on vertical walls, *Chem. Eng. Sci*., **102**, 585-601.

Wang, T., Davidson, J.F. and Wilson, D.I. (2014) Flow patterns and cleaning behaviour of horizontal liquid jets impinging on angled walls, submitted to *Food Bioproducts Proc*.

Wilson, D.I. (2005) Challenges in cleaning: Recent developments and future prospects, *Heat Transfer Engineering*, **26**(1), 51-59.

Wilson, D.I., Atkinson, P., Köhler, H., Mauermann, M., Stoye, H., Suddaby, K., Wang, T., Davidson, J.F. and Majschak, J-P. (2014) Cleaning of soft-solid soil layers on vertical and horizontal surfaces by coherent impinging liquid jets, *Chem. Eng. Sci*., **109**, 183–196.

Wilson, D.I., Le, B.L., Dao, H.D.A., Lai, K.Y., Morison, K.R. and Davidson, J.F. (2012) Surface flow and drainage films created by horizontal impinging liquid jets, *Chem. Eng. Sci*., **68**, 449–460.

Yeckel, A, and Middleman, S. (1987). Removal of a viscous film from a rigid plane surface by an impinging liquid jet, *Chem. Eng. Comm*., **50**, 165-167.

Nomenclature

Roman

a	radial location of cleaning front	m
a_c	radius of circular cleaned region in stationary model	m
a_i	radius when cleaning front is first seen	m
a_x	radial location of cleaning front on jet path	m
c	lumped parameter, Equation [2]	$kg^2\ m^{-4}\ s^{-1}$
C_d	nozzle discharge coefficient	-
d_N	nozzle throat diameter	m
E_E	energy consumption performance indicator	$kg\ J^{-1}$
E_t	time-based cleaning performance indicator	$kg\ s^{-1}$
E_v	liquid consumption performance indicator	$kg\ m^{-3}$
k	cleaning rate constant, Equation [2]	not defined
k'	lumped cleaning rate constant	$m\ s\ kg^{-1}$
K	lumped parameter, Equation [7]	
M	momentum flux per unit width	$kg\ s^{-2}$
$\dot{m}$	mass flow rate	$kg\ s^{-1}$
m_0	mean surface mass coverage	$kg\ m^{-2}$
p	radial distance to cleaning front, Equation [10]	m
ΔP	pressure difference across nozzle	Pa
R^2	correlation coefficient	-
r	radial co-ordinate	m
r_o	jet radius	m
R_F	radius of film jump at mid-plane	m
R_H	radius of hydraulic jump	m
Re_{jet}	jet Reynolds number, defined $Re_{jet} = \rho U_o d_N/\mu$	-
t	time	s
Δt	total time after cleaning front is first seen, $= t - t_i$	s
t_i	time at which cleaning front is first seen	s
U	mean velocity in film	$m\ s^{-1}$
U_o	jet and initial film mean velocity	$m\ s^{-1}$
v_{jet}	nozzle traverse speed	$m\ s^{-1}$

W	draining film width	m
w_c	width of cleaned region	m
x	Cartesian co-ordinate	m
y	Cartesian co-ordinate	m
Z	height of inner radial zone above the point of impingement	m

Greek

α	Constant, Equation [9]	$m^5 s^{-1}$
β	contact angle	^{o}
δ	thickness of layer	m
γ	surface tension (liquid/vapour)	$N m^{-1}$
μ	dynamic viscosity	Pa s
θ	azimuthal angle	^{o}
ϕ	orientation of cleaning vector	^{o}
ρ	density	$kg m^{-3}$

Table 1 Summary of experimental studies

Nozzle diameter	Discharge coefficient	Feed pressure	Nozzle Traverse speed	Jet velocity range	Jet Reynolds number
d_N mm	C_d -	ΔP barg	v_{jet} mm s^{-1}	U_o m s^{-1}	Re_{jet} -
0.84	0.94	0.5, 1.0, 1.5, 2.0	2.1, 10.5, 21, 50.4	9.45 ~ 18.9	7 700 ~ 15 400
1.03	0.95	1.0, 1.5, 2.0, 3.0	2.1, 10.5, 21, 42	13.5 ~ 23.3	13 500 ~ 23 300
1.69	0.96	0.5, 1.0, 1.5, 2.0	2.1, 10.5, 21, 50.4, 75.6, 84, 92.4, 100.8, 105, 126	9.66 ~ 19.3	15 800 ~ 31 600
2.66	0.97	0.5, 1.0, 1.5, 2.0	2.1, 10.5, 21, 50.4	9.71 ~ 19.4	25 000 ~ 50 100

Figure captions

Figure 1 Flow patterns created by (*a*) vertical jet impinging on horizontal plate to give a hydraulic jump, radius R_H, and (*b*) horizontal jet impinging on vertical plate to give a film jump, circumferential rope and falling film. O marks the point of impingement. Grey lines show liquid flow pattern; dashed line indicates location of jump. R_F is the radius of the film jump at the midplane, while Z is the height of the jump above the point of impingement, with $Z < R_F$.

Figure 2 Evolution of size of cleaned area in tests with stationary water jets impinging downwards on horizontal substrates coated with 1.3 mg cm^{-2} Xanthan gum/ZnS layer, plotted in the form predicted by Equation [7]. Water feed pressure 1.5 barg. Solid symbols indicate that $a_c < R_H$; open symbols denote that the cleaned region had extended beyond the hydraulic jump, *i.e.* $a_c > R_H$.

Figure 3 (*a*) Photograph and (*b*) schematic of cleaned region for an interrupted experiment where a vertical water jet was moving across a coated plate from left to right. The frame of reference in (*a*) is the laboratory, whereas in (b) it is the point of jet impingement, O. Layer appears green under UV illumination: cleared region is black. Video available as Supplementary Material. Conditions: feed pressure 1.5 barg, d_N = 1.69 mm, v_{jet} = 10.5 mm s^{-1}; Xanthan gum/ZnS coverage 1.1 mg cm^{-2}.

Figure 4 Vector diagram for cleaning front at point P in Figure 3(*b*). Narrow solid lines denote displacement vectors: broad solid lines are velocity vectors.

Figure 5 Predicted shape of cleaning front obtained by integrating Equation [12]. Locus plotted in Cartesian co-ordinates, relative to the point of impingement O (see Figure 3(*b*)). Superimposed on the locus are data sets obtained from interrupted experiments, scaled using Equation [13] to identify a_x from w_c. Point W is the location of the maximum in cleared region width predicted by the model, located a distance p_W from the point of impingement O. Conditions: ΔP = 1.5 bar, v_{jet} = 10.5 mm s^{-1}, d_N = 1.69 mm. Flow stopped after (A) 30 cm nozzle travel, m_0 = 1.16 mg cm^{-2}; (B) 10 cm travel, m_0 = 1.38 mg cm^{-2}. Dotted circle shows locus of a circle of radius a_x.

Figure 6. Schematic of cleaning test rig showing moving nozzle and monitoring system

Figure 7. Photograph of cleaned plate with solid white lines showing edge detection within the region of interest (denoted by dotted lines). Test conditions: d_N = 1.69 mm, ΔP = 1.5 barg, v_{jet} = 2.1 mm s^{-1}, giving w_c = 63.5 mm.

Figure 8 Comparison of mean velocity in the liquid film, evaluated at the nose of the cleaning front, with the traversing jet velocity. Experimental conditions summarised in Table 1.

Figure 9 Figure 9 Ratio of p_w (see Figure 5) to the estimated radius of the radial flow region, R_H.

Figure 10 Comparison of experimental data with Equation [15]. Solid symbols indicate data which satisfy $p_W < R_H$. Open symbols indicate data where $p_W > R_H$. Dashed line shows fit of Equation [15] to solid symbols, with R^2 = 0.846. E marks data for d_N = 1.69 mm, high v_{jet}, where the model gives poor prediction.

Figure 11 Effect of design parameters on predicted nozzle cleaning performance indicators. Each datum represents a combination of ΔP, d_N and v_{jet}. Point S is the reference configuration, with ΔP = 1.5 bar, d_N = 1.69 mm and v_{jet} = 21 mms^{-1}. Loci show results for varying one design

parameter while the other two are held constant, with (*i*) $2 \le v_{jet} \le 130$ mm s^{-1}; (*ii*) $0.5 \le \Delta P \le 5.0$ bar; (*iii*) $0.39 \le d_N \le 3.3$ mm.

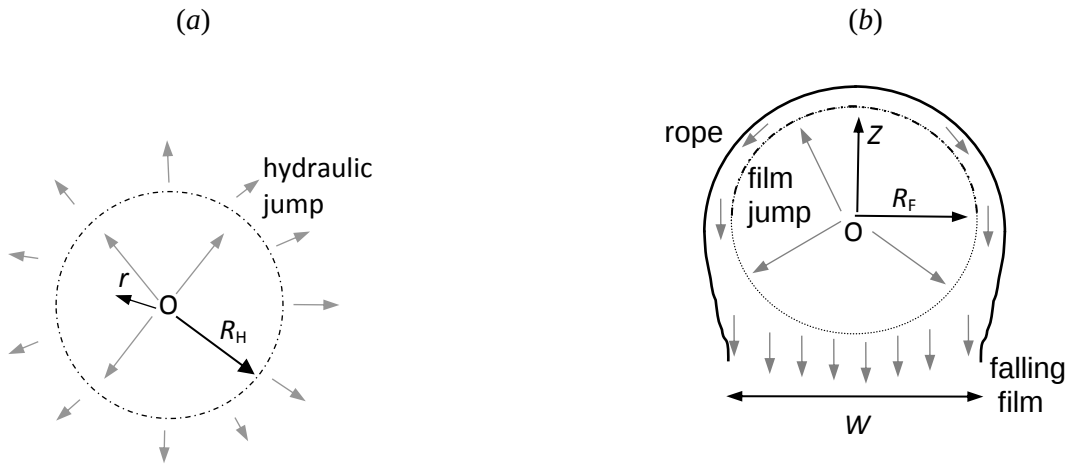

Figure 1 Flow patterns created by (*a*) vertical jet impinging on horizontal plate to give a hydraulic jump, radius R_H, and (*b*) horizontal jet impinging on vertical plate to give a film jump, circumferential rope and falling film. O marks the point of impingement. Grey lines show liquid flow pattern; dashed line indicates location of jump. R_F is the radius of the film jump at the midplane, while Z is the height of the jump above the point of impingement, with $Z < R_F$.

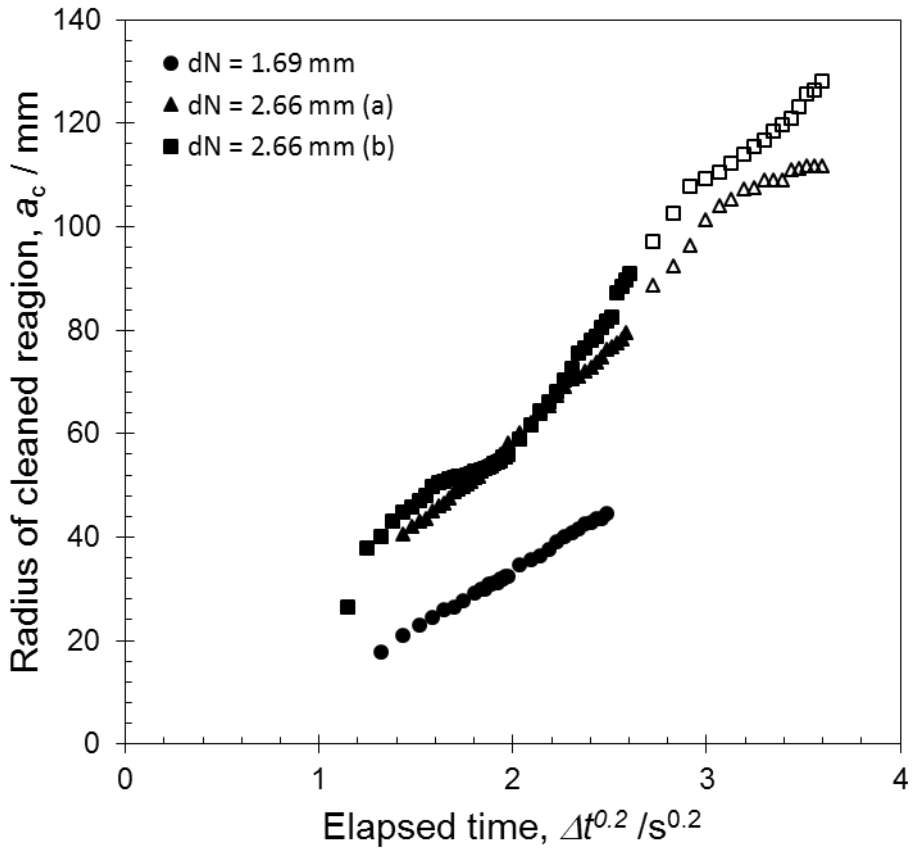

Figure 2 Evolution of size of cleaned area in tests with stationary water jets impinging downwards on horizontal substrates coated with 1.3 mg cm^{-2} Xanthan gum/ZnS layer, plotted in the form predicted by Equation [7]. Water feed pressure 1.5 barg. Solid symbols indicate that $a_c < R_H$; open symbols denote that the cleaned region had extended beyond the hydraulic jump, *i.e.* $a_c > R_H$.

(*a*)

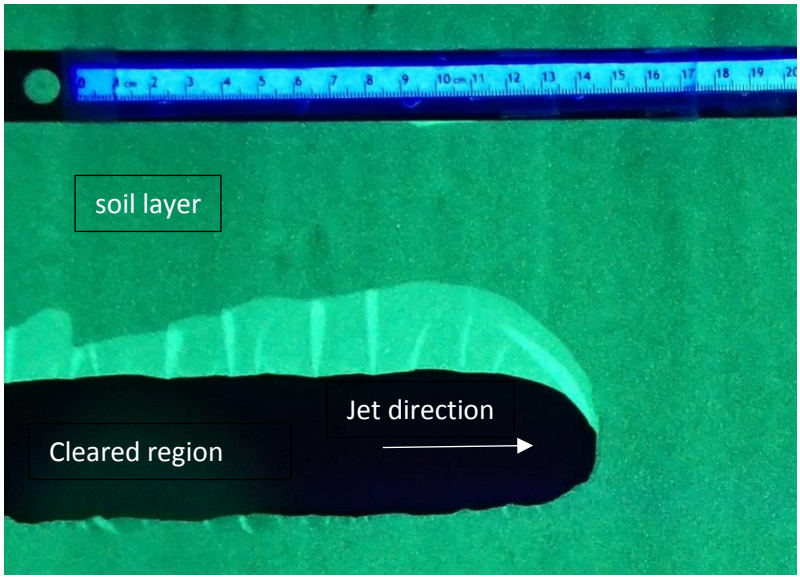

(*b*)

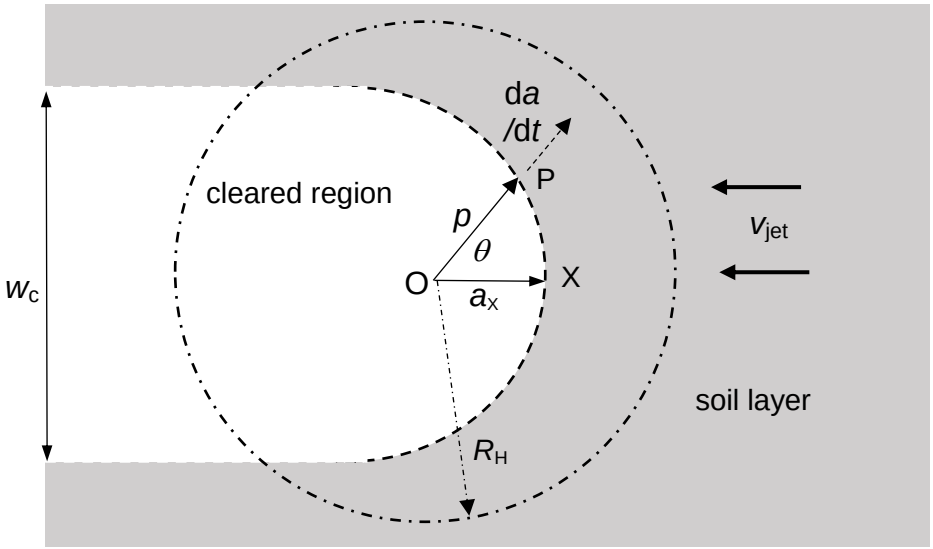

Figure 3 (*a*) Photograph and (*b*) schematic of cleaned region for an interrupted experiment where a vertical water jet was moving across a coated plate from left to right. The frame of reference in (*a*) is the laboratory, whereas in (b) it is the point of jet impingement, O. Layer appears green under UV illumination: cleared region is black. Video available as Supplementary Material. Conditions: feed pressure 1.5 barg, d_N = 1.69 mm, v_{jet} = 10.5 mm s^{-1}; Xanthan gum/ZnS coverage 1.1 mg cm^{-2}.

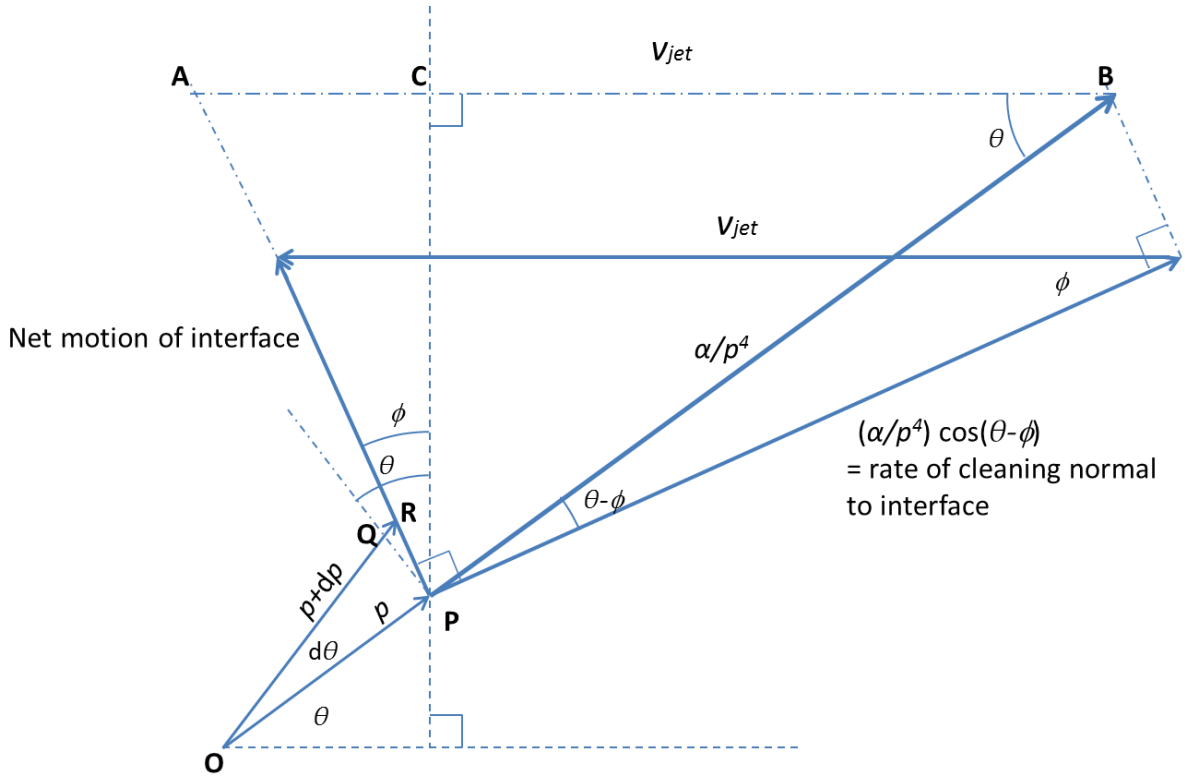

Figure 4 Vector diagram for cleaning front at point P in Figure 3(*b*). Narrow solid lines denote displacement vectors: broad solid lines are velocity vectors.

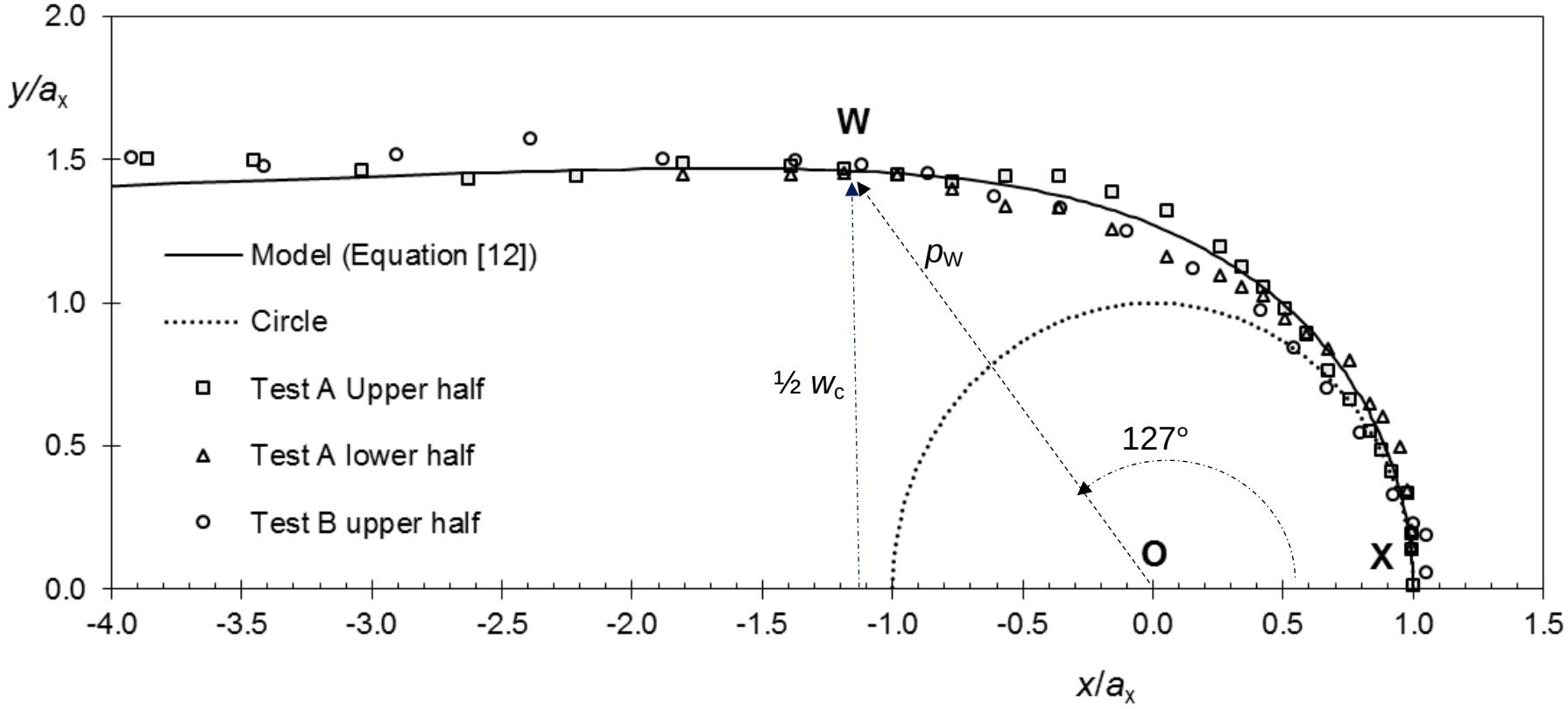

Figure 5 Predicted shape of cleaning front obtained by integrating Equation [12]. Locus plotted in Cartesian co-ordinates, relative to the point of impingement O (see Figure 3(*b*)). Superimposed on the locus are data sets obtained from interrupted experiments, scaled using Equation [13] to identify a_x from w_c. Point W is the location of the maximum in cleared region width predicted by the model, located a distance p_W from the point of impingement O. Conditions: ΔP = 1.5 bar, v_{jet} = 10.5 mm s^{-1}, d_N = 1.69 mm. Flow stopped after (A) 30 cm nozzle travel, m_0 = 1.16 mg cm^{-2}; (B) 10 cm travel, m_0 = 1.38 mg cm^{-2}. Dotted circle shows locus of a circle of radius a_x.

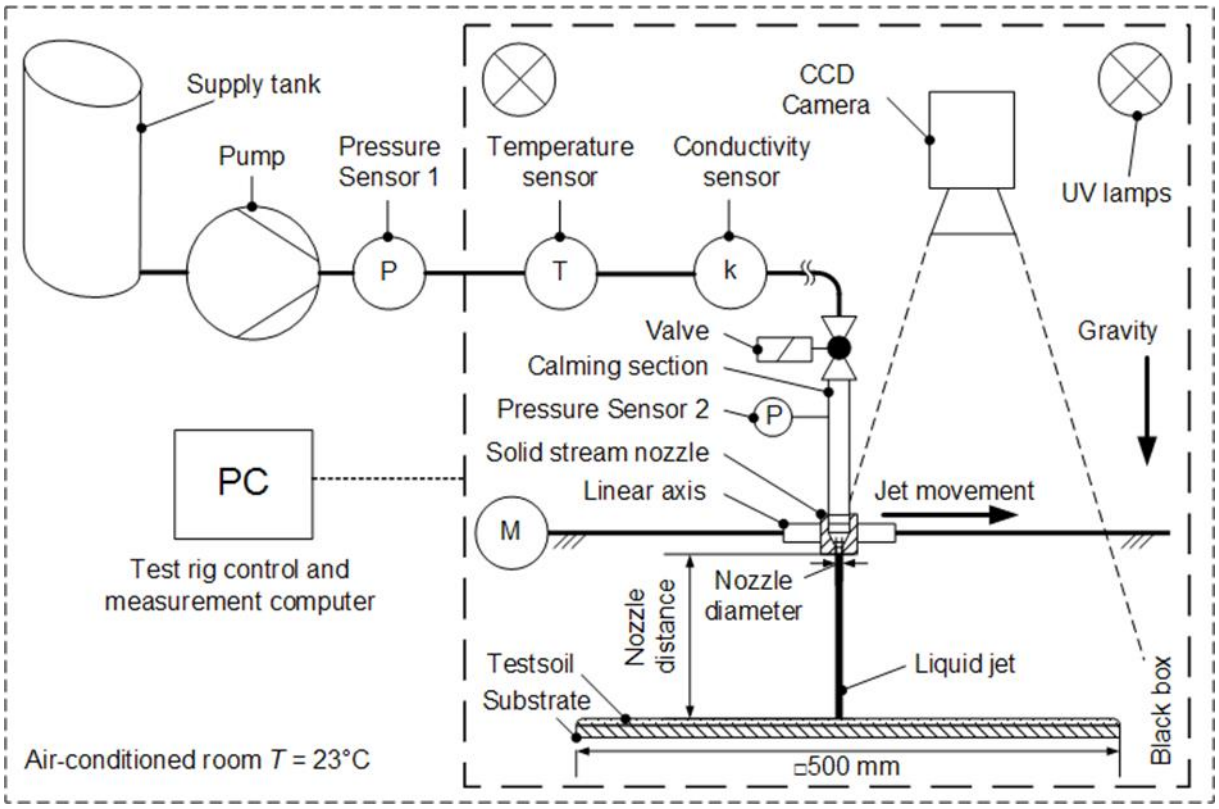

Figure 6. Schematic of cleaning test rig showing moving nozzle and monitoring system

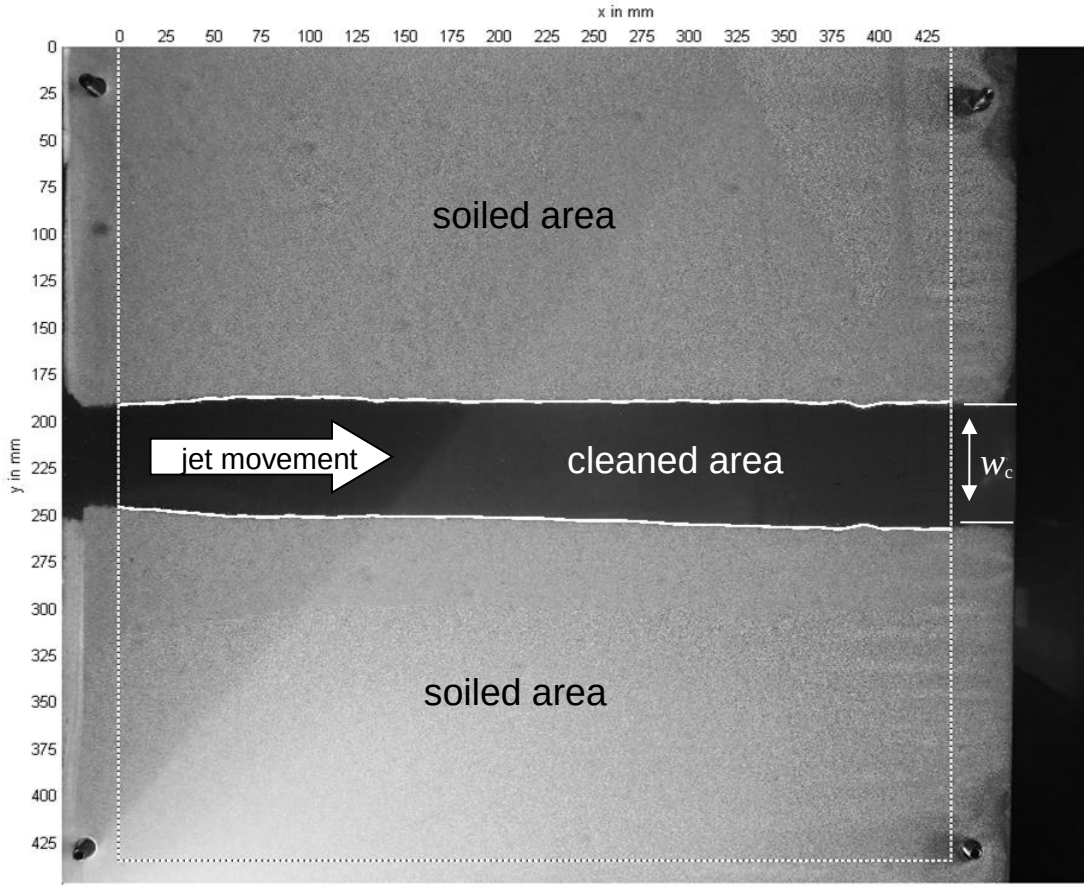

Figure 7. Photograph of cleaned plate with solid white lines showing edge detection within the region of interest (denoted by dotted lines). Test conditions: $d_N = 1.69$ mm, $\Delta P = 1.5$ bar, $v_{jet} = 2.1$ mm s^{-1}, giving $w_c = 63.5$ mm.

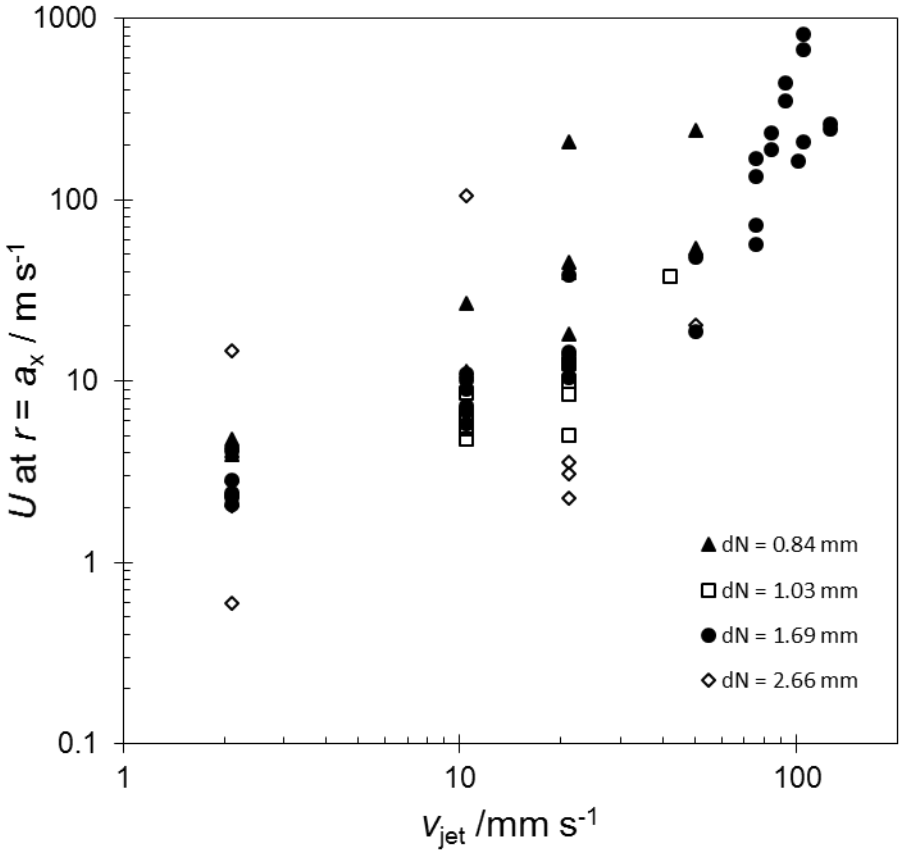

Figure 8 Comparison of mean velocity in the liquid film (in m s^{-1}), evaluated at the nose of the cleaning front, with the traversing jet velocity (in mm s^{-1}). Experimental conditions summarised in Table 1.

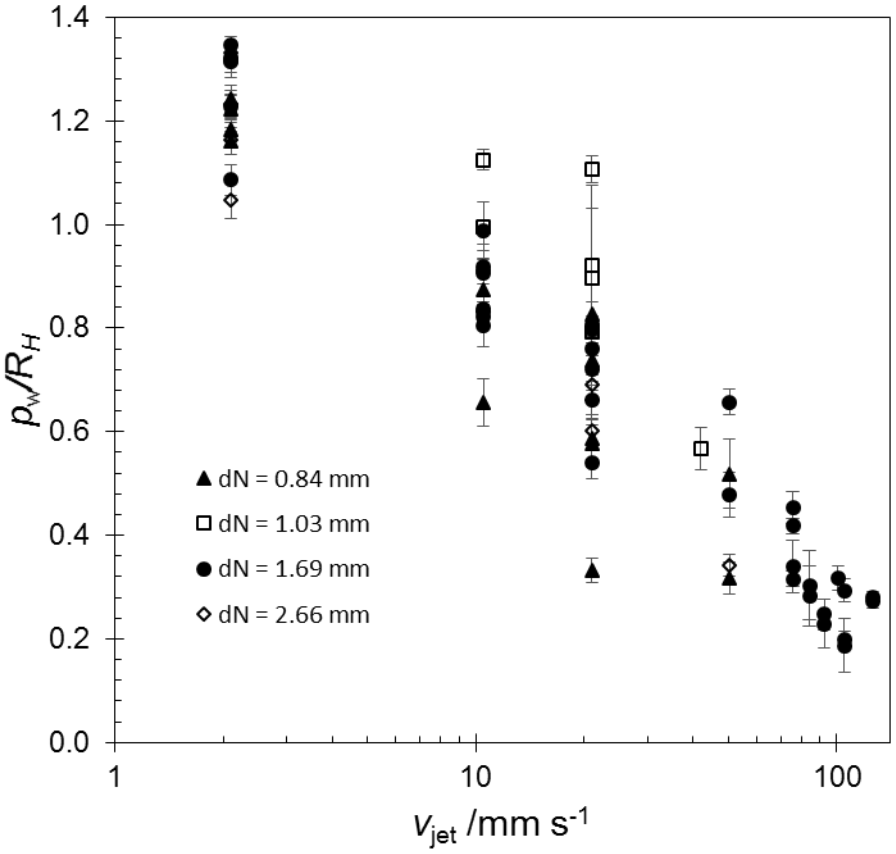

Figure 9 Ratio of p_w (see Figure 5) to the estimated radius of the radial flow region, R_H.

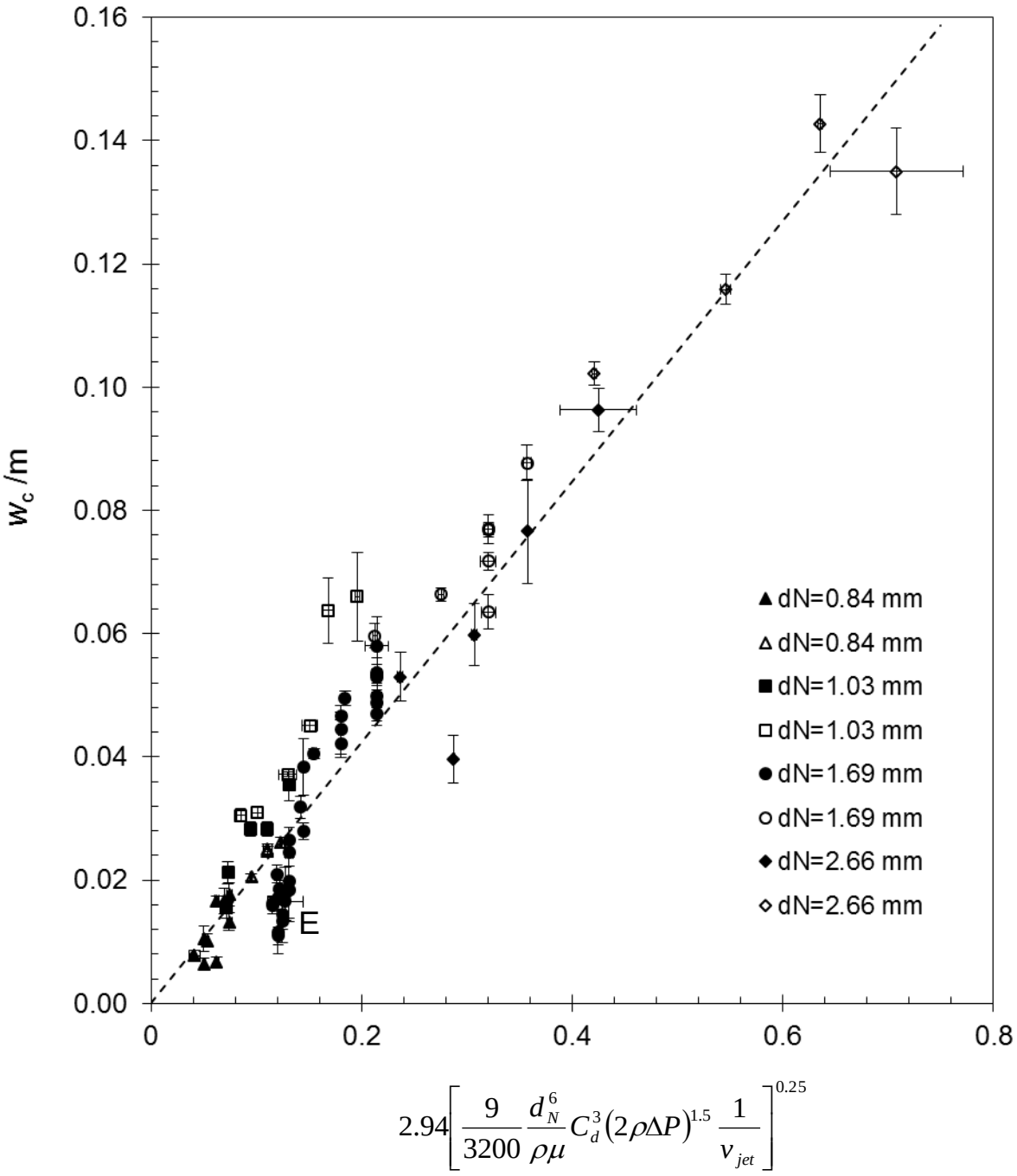

Figure 10 Comparison of experimental data with Equation [15]. Solid symbols indicate data which satisfy $p_W < R_H$. Open symbols indicate data where $p_W > R_H$. Dashed line shows fit of Equation [15] to solid symbols, with $R^2 = 0.846$. E marks data for $d_N = 1.69$ mm, high v_{jet}, where the model gives poor prediction.

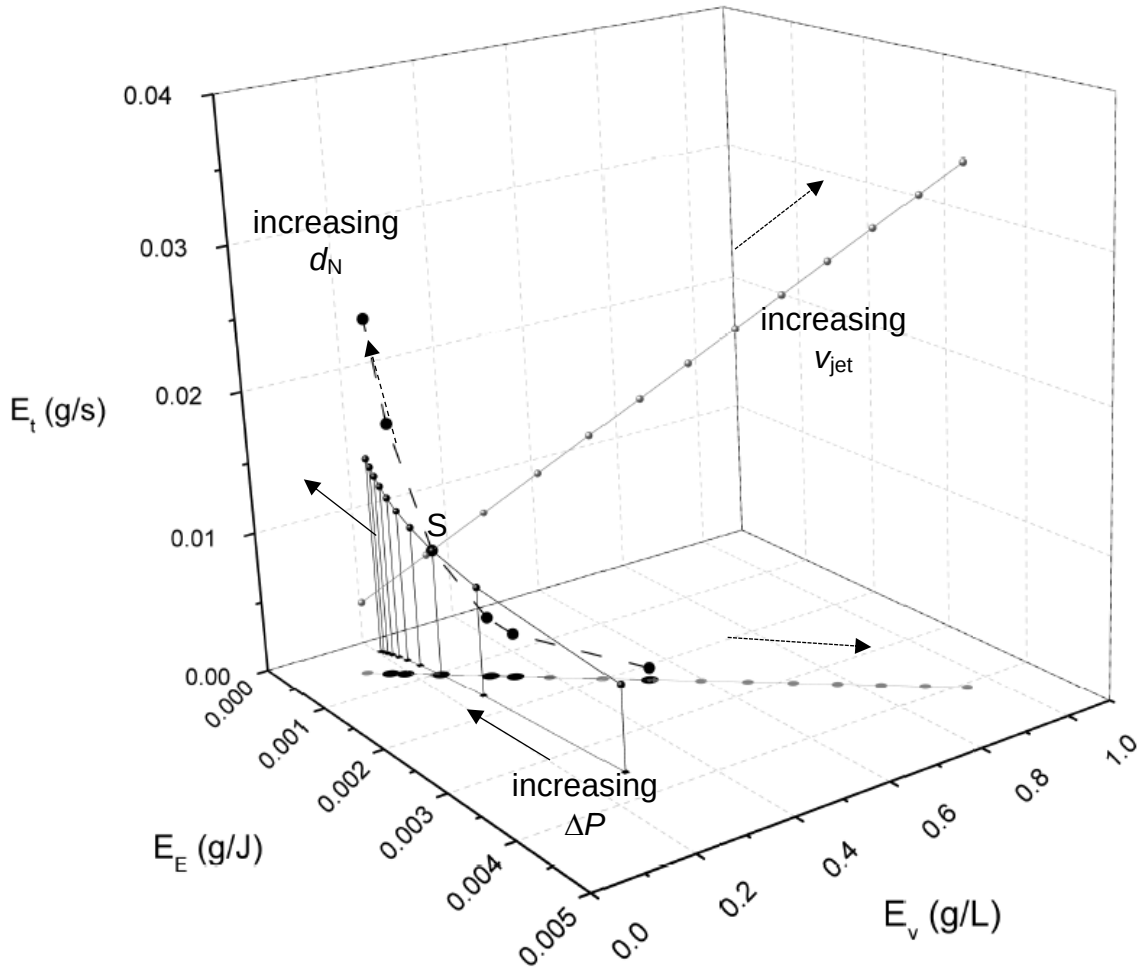

Figure 11 Effect of design parameters on predicted nozzle cleaning performance indicators. Each datum represents a combination of ΔP, d_N and v_{jet}. Point S is the reference configuration, with ΔP = 1.5 bar, d_N = 1.69 mm and v_{jet} = 21 mms^{-1}. Loci show results for varying one design parameter while the other two are held constant, with (*i*) $2 \leq v_{jet} \leq 130$ mm s^{-1}; (*ii*) $0.5 \leq \Delta P \leq 5.0$ bar; (*iii*) $0.39 \leq d_N \leq 3.3$ mm.